

Fluxoid fluctuations in mesoscopic superconducting rings

Julie A. Bert, Nicholas C. Koshnick, Hendrik Bluhm,^{*} and Kathryn A. Moler[†]

Department of Physics and Department of Applied Physics, Stanford University, Stanford, California 94305, USA

(Received 27 August 2010; revised manuscript received 27 April 2011; published 18 October 2011)

Superconducting rings represent an ideal system for studying phase coherence in one dimension. We study the temperature dependence of the magnetic susceptibility of superconducting rings with a scanning superconducting quantum interference device. The physical parameters of the rings were designed to reduce the superconducting phase stiffness. We observe a suppression of the susceptibility signal below the critical temperature, which we attribute to a thermodynamic sampling of metastable states with different phase winding number, termed fluxoid fluctuations. We introduce a simple model (N. C. Koshnick, Ph.D. thesis, Stanford University, 2009) for the susceptibility of a ring affected by fluxoid fluctuations and compare it with one-dimensional (1D) Ginzburg-Landau (GL) theory including all thermal fluctuations. We find good agreement between our fluxoid model and the full 1D GL theory up to a shift in the critical temperature. Additionally, our magnetic susceptibility data are well described by 1D GL theory.

DOI: 10.1103/PhysRevB.84.134523

PACS number(s): 73.23.Ra, 74.40.-n, 74.25.Ha

I. INTRODUCTION

In this paper, we study the properties of superconducting one-dimensional (1D) wires in a model system: uniform isolated aluminum rings. Superconducting rings have states with uniform phase windings that differ by integer multiples of 2π , called fluxoid states. Phase slips allow for transitions between fluxoid states. During a phase slip the order parameter phase loses or gains a twist by suppressing superconductivity in a portion of the ring. Phase slips are detected as jumps in measurable quantities such as the current. In contrast, fluxoid fluctuations represent the thermal occupation of different fluxoid states. Their impact on the ring's current is represented by a thermodynamic sampling of all energetically accessible fluxoid states. By generating a Boltzmann distribution of these fluxoid states, Koshnick formulated a model¹ that predicts a suppression in the temperature dependence of the ring's zero-field magnetic susceptibility. Complementing previous experiments that studied amplitude fluctuations in rings with long mean free paths,^{2,3} we present experimental data from short-mean-free-path rings which exhibit a downturn in the susceptibility close to the critical temperature. Moreover, we show that our fluxoid fluctuation model provides a good fit to the susceptibility data. This paper is not intended to be a complete review of superconducting fluctuations in reduced dimensions. We restrict our analysis to thermal fluctuations of the Ginzburg-Landau (GL) order parameter that are described by 1D GL theory. We do not treat quantum fluctuations or Langevin noise and we assume our rings are homogeneous.

Fluctuations play an important role in the superconducting behavior of samples of reduced dimensionality:⁴ they can make electron pairing and long-range phase coherence occur at different temperatures in unconventional superconductors,⁵ lead to the Berezinskii-Kosterlitz-Thouless transition⁶ in two dimensions, cause the destruction of long-range phase order in infinitely long one-dimensional wires,⁷ and determine the resistive properties of 1D wires of finite length.^{8–11}

The nature of superconducting fluctuations in rings has generated significant interest. Fluxoid dynamics in individual rings have been probed as a function of ring size,^{12–14} magnetic field,^{13,15,16} and temperature.^{14,17,18} The occupation of

metastable fluxoid states has also been measured to determine a crossover from 1D to 2D behavior in wide rings.^{19,20} Phase slip rates have been studied in both conventional low- T_c (Ref. 3) and unconventional high- T_c (Ref. 21) superconducting rings. Ring inhomogeneities, such as weak links or nonuniform widths, have been studied as phase slip sites that can impact the ring's current-phase relationship and fluxoid transitions.^{16,22–26}

Transport measurements have long been used as a probe of superconducting fluctuations.^{27,28} Transport measures voltage, which is directly related to the phase slip rate. In contrast, we use a scanning superconducting quantum interference device (SQUID) to make a magnetic measurement that is sensitive to the thermodynamic equilibrium current in the ring. Specifically, we measure the effects of superconducting fluctuations on the ring's equilibrium supercurrent I as a function of applied flux Φ_a , measured in a temperature range near the critical temperature T_c . Direct measurements of the ring current as a function of applied flux are useful because they provide access to the thermodynamic free energy through the derivative $I = -\partial F/\partial\Phi_a$. While there are also interesting features in the full flux dependence,² in this paper we measure the ring's zero-field susceptibility as a function of temperature, $dI(T)/d\phi|_{\phi=0}$, where $\phi = \Phi_a/\Phi_0$ and $\Phi_0 = h/2e$ is the superconducting flux quantum.

Theoretical work using Ginzburg-Landau theory has predicted the current in the presence of an applied flux threading the ring. Ambegaokar and Eckern applied a Gaussian approximation to GL theory to predict a mesoscopic persistent current driven by superconducting fluctuations above T_c .^{29,30} However, the Gaussian approximation, accurate far above T_c where the quadratic term in the GL free energy dominates, diverges as T approaches T_c . von Oppen and Riedel formulated a transfer matrix approach to GL theory that accounts for all thermal fluctuations to calculate the supercurrent and correct the divergence at T_c .³¹ More recently, Schwiete and Oreg proposed a simplification of the full formulation by von Oppen and Riedel (VOR) that makes an analytic prediction for the ring's susceptibility $dI/d\Phi_a$ in the limit where the superconducting coherence length is of the order of the radius.³² Schwiete and Oreg provide a simple alternative to

solving the VOR model numerically. This model is applicable to long-mean-free-path rings with a short circumference, rather than the short-mean-free-path rings with long circumferences discussed in this paper.

A number of different experiments have used current and susceptibility measurements to study fluctuations in individual superconducting rings.^{2,3,14,23,33} Zhang and Price studied the phase slip rate and susceptibility as a function of temperature in a single Al ring.³ The ring's geometry and long mean free path favored amplitude fluctuations that were expected to support a susceptibility response above T_c . However, the observed susceptibility signal was an order of magnitude larger than predicted by GL theory. Koshnick *et al.*² measured the susceptibility of 15 individual rings with long mean free paths as a function of Φ_a . All rings showed a fluctuation-induced susceptibility response above T_c , which agreed well with complete 1D GL theory.³¹

This paper focuses on rings with shorter mean free paths and longer circumferences, which should exhibit fluxoid fluctuations. Instead of generating an enhancement in the susceptibility above T_c , fluxoid fluctuations can suppress the ring's superconducting response well below T_c . We start in Sec. II A by describing the different thermal fluctuations experienced by our rings, and establish the physical conditions that support fluxoid fluctuations. We outline a model,¹ derived from the 1D GL free energy functional, where a thermal distribution of fluxoid states suppresses the rings' diamagnetism (Sec. II C). Our theoretical analysis concludes by comparing our fluxoid model to a complete theory that includes all thermal fluctuations in the GL framework³¹ (Sec. II D). We find good agreement between the models in rings with short mean free paths where fluxoid fluctuations dominate the response. Finally, we discuss our measurement technique in Sec. III and present data from two sets of ring samples, which are well described by our 1D GL models (Sec. III C).

II. FLUCTUATION THEORY

A. Types of fluctuations

GL theory introduces a complex order parameter $\psi(\mathbf{r})$ with an associated amplitude and phase. Fluctuations are deviations in ψ from the mean-field solutions corresponding to local minima of the GL free energy functional, which affect the order parameter's amplitude or phase. Fluctuations become significant when the thermal energy of the system allows multiple wave functions to contribute to the ring's response. When multiple fluxoid states are thermally accessible even at zero applied flux, the ring fluctuates between its minimum-energy fluxoid state and the metastable fluxoid states, a process we call fluxoid fluctuations. In addition to fluxoid fluctuations, 1D GL theory accounts for fluctuations in the amplitude of the superconducting order parameter and phase fluctuations that are not uniform around the ring. The main difference between our fluxoid model presented in Sec. II C and the full 1D GL theory formulated by Von Oppen and Riedel (Sec. II D) is that the latter includes these amplitude and nonuniform phase fluctuations.

It is important at this point to emphasize the distinction between phase slips and fluxoid fluctuations. Fluxoid fluctuations

represent equilibrium phenomena and will not be observable on measurement time scales if the ring is not experiencing phase slips which populate higher phase winding states. The next three sections lay out and compare the energy scales for the onset of both fluxoid fluctuations and phase slips.

1. Fluxoid fluctuations

The ring geometry of our samples imposes a constraint on the order parameter phase. The order parameter phase must be single valued modulo 2π ; therefore the cylindrical symmetry of the system results in a phase that winds by an integer multiple of 2π around the ring. Each fluxoid state, with free energy F_n and phase winding $2\pi n$, represents a stable local minima of the GL free energy functional.

We start by finding expressions for F_n . One-dimensional Ginzburg-Landau theory introduces the GL free energy functional in the presence of a magnetic field represented by the vector potential \vec{A} ,

$$F[\psi(x)] = \int \left[\alpha |\psi(x)|^2 + \frac{1}{2} \beta |\psi(x)|^4 + \frac{\hbar}{2m^*} \left| \left(\vec{\nabla} - \frac{ie^*\vec{A}}{\hbar} \right) \psi(x) \right|^2 \right] d^3x. \quad (1)$$

α and β both depend on T , and $\alpha^2/\beta = B_c(T)^2/\mu_0$ is related to the superconducting critical field $B_c(T)$. e^* and m^* are the charge and mass of the Cooper pairs and μ_0 is the permeability of free space.

We look for stable solutions that locally minimize the Ginzburg-Landau free energy functional. In a homogeneous one-dimensional ring fluxoid states have free energies

$$F_n(T, \phi) = -F_c(T) \left(1 - \frac{\xi(T)^2}{R^2} (\phi - n)^2 \right)^2, \quad (2)$$

where the critical field and the ring volume ($V = 2\pi Rwd$) determine the ring's total condensation energy [$F_c(T) = VB_c(T)^2/2\mu_0$]. w is the ring width and d is the thickness. The dependence on $\xi(T)/R$ accounts for the suppression of the superfluid density by the phase gradient around the ring with coherence length $\xi(T)$ and radius R . The applied flux $\phi = \Phi_a/\Phi_0$ can be transformed into a shift in the boundary conditions for a wave function in a ring,³⁴ and therefore contributes to the energy in the same way as n .

We approximate the energy associated with each fluxoid state by expanding the mean-field GL free energy expression, Eq. (2), to lowest order in $\xi(T)/R$. The energy difference between the lowest-energy fluxoid states at zero applied flux,

$$\begin{aligned} \Delta F_{\pm 1,0}(T, \phi = 0) &= F_{\pm 1}(T, \phi = 0) - F_0(T, \phi = 0) \\ &\approx 4\pi\xi wd \frac{B_c^2}{2\mu_0} \frac{\xi}{R}, \end{aligned} \quad (3)$$

is indicated with a red arrow in Fig. 1. This energy barrier determines the onset of fluxoid fluctuations in our zero-field susceptibility measurements presented in Sec. III.

2. Phase slips

A phase slip is the process of changing the fluxoid number by 2π by briefly driving the order parameter amplitude to zero

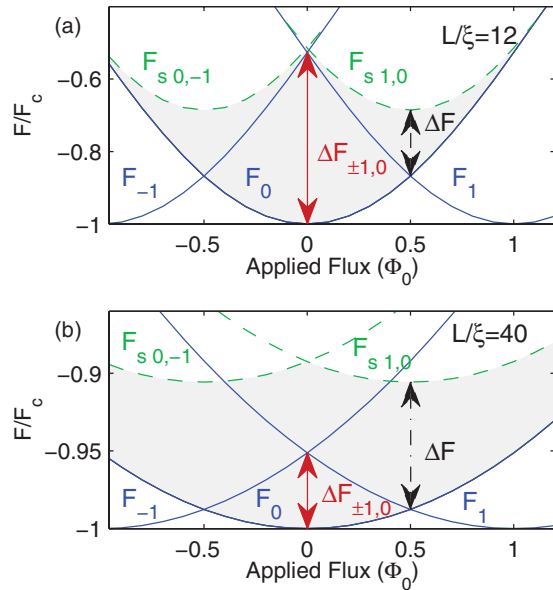


FIG. 1. (Color online) (a),(b)Free energy of fluxoid states [blue solid line, Eq. (2)] and saddle point energies [green dashed line, Eq. (4)] as a function of applied flux, in units of the condensation energy F_c . The energy barrier between adjacent fluxoid states at zero applied flux, $\Delta F_{\pm 1,0}$, is indicated by the solid red arrow. The saddle point energy barrier for phase slips is a flux-dependent quantity indicated by the gray-shaded region. The saddle point barrier at $\phi = 1/2$, indicated by the black dashed arrow, sets the condition for thermal equilibrium.

in a coherence-length-sized section of the ring.⁴ The phase slip activation energy is found by calculating the lowest-energy pathway between two fluxoid states as defined by the energy barrier for the saddle point in wave function configuration space. The saddle point energies F_{sn} , being stationary points of the free energy, must also satisfy the GL equations; however, these solutions represent unstable configurations. We find an approximate condition for the onset of phase slips from calculations of the energy barrier.

Langer and Ambegaokar were the first to use 1D GL theory to calculate the saddle point free energy barrier between fluxoid states in 1D wires where the wire length was much greater than the superconducting coherence length.⁸ Zhang modified Langer and Ambegaokar's solution for a ring geometry,³⁵ and found the saddle point energy in rings where $L \gg \xi(T)$:

$$F_{sn}(T, \phi) = F_c(T) \left(\frac{8\sqrt{2\delta(T, \phi, n)} \xi(T)}{3} - \frac{[2 + \delta(T, \phi, n)]^2}{9} \right), \quad (4)$$

where $L = 2\pi R$ is the ring's circumference and $\delta(T, \phi, n)$ is the normalized difference between the squares of the order parameter amplitudes near and far from a phase slip event. $\delta(T, \phi, n)$ is a real number between 0 and 1 that satisfies the relation

$$2\pi n = \sqrt{\frac{1-\delta}{3}} \frac{L}{\xi(T)} + 2 \tan^{-1} \left(\sqrt{\frac{3\delta}{2(1-\delta)}} \right) + 2\pi\phi. \quad (5)$$

For $\phi = n + 1/2$, $\delta = 1$.

We are interested in a regime where $L \gg \xi(T)$, and δ remains close to 1 for moderate n . Using the substitution $\kappa = \sqrt{1-\delta}$ and expanding to lowest order in κ , we arrive at a simplified expression for δ :

$$\delta(T, \phi, n) = 1 - \left(\frac{\sqrt{3}\pi(2n - 2\phi - 1)}{\frac{L}{\xi(T)} - 2\sqrt{2}} \right)^2. \quad (6)$$

Extending the $L \gg \xi$ limit allows us to set $\delta \approx 1$. This approximation makes $F_{sn}(T, \phi) = F_{sn}(T)$ independent of flux. We can now calculate the free energy barrier for phase slips as a function of applied flux $\Delta F_{s\pm 1,0}(T, \phi)$, for a ring that starts in the $n = 0$ fluxoid state and transitions to the $n = \pm 1$ state:

$$\Delta F_{s\pm 1,0}(T, \phi) = [F_{s\pm 1}(T) - F_0(T, \phi)] \approx \xi w d \frac{B_c^2}{2\mu_0} \left(\frac{8\sqrt{2}}{3} - 4\pi \frac{\xi}{R} \phi^2 \right). \quad (7)$$

This energy barrier depends on the applied flux and is indicated by the gray-shaded region in Fig. 1. In the limit where $L \gg \xi$, the second term in Eq. (7) can be ignored, and the energy barrier no longer depends on flux.

3. Comparison of energy scales

In Fig. 1, the energy expressions for the fluxoid states, Eq. (2), blue solid line, and the saddle point states, Eq. (4), green dashed line, for two rings with different L/ξ are plotted as functions of flux and fluxoid number n . The solid red arrow indicates the energy barrier for fluxoid fluctuations at $\phi = 0$, Eq. (3). It is the energy difference between consecutive fluxoid states. The shaded area shows the flux-dependent energy barrier for phase slips between the $n = 0$ and the $n = \pm 1$ fluxoid states, Eq. (7). This is the energy difference between the fluxoid state and the saddle point state. The figure demonstrates how the energy barrier for phase slips decreases with increasing applied flux.

Our magnetic susceptibility data points are generated by extracting the slope at zero field of the current response of a ring threaded by magnetic flux, where the applied flux is swept through several flux quanta. We are interested in the energy barrier for fluxoid fluctuations at $\phi = 0$, because we expect those fluctuations to affect our zero-field susceptibility signal.

Since fluxoid fluctuations represent a thermodynamic sampling of fluxoid states, this description is only valid in thermal equilibrium when frequent phase slips populate higher phase winding states. At low temperatures, if the applied flux is swept through the entire range presented in Fig. 1, then the lowest saddle point energy barrier, found at the ends of the flux range, determines the onset of phase slips. In this case the ring will be hysteretic, or even exhibit no transitions if the barrier for phase slips remains large compared to the thermal energy over the entire flux range.

In thermal equilibrium the ring has sufficient thermal energy to make a transition at every crossing of the phase winding state, and there is no hysteresis in the forward and backward field sweeps. Consequently phase slips must be energetically favorable at each value of $\phi = n + 1/2$. Therefore the condition for equilibrium requires the thermal energy to be greater than the energy barrier for phase slips at $\phi = 1/2$, indicated by the black dashed arrow in Figs. 1(a) and 1(b).

Fluxoid fluctuations will suppress the thermal equilibrium ring response if the energy barrier for fluxoid fluctuations is also small compared the temperature. For example, the ring in Fig. 1(a) has a larger barrier for fluxoid fluctuations at $\phi = 0$ than for phase slips at $\phi = 1/2$. As the temperature is increased, phase slips will drive the ring into thermal equilibrium before the temperature where fluxoid fluctuations suppress the response. The ring in Fig. 1(b) is in the opposite limit; the barrier for fluxoid fluctuations at $\phi = 0$ is smaller than the thermal equilibrium barrier for phase slips. In this ring fluxoid fluctuations will not be apparent on the measurement time scale until phase slips allow the ring to enter thermal equilibrium.

B. Phase slips and equilibrium

The ring is in thermal equilibrium when the thermal energy is greater than the phase slip energy at $\phi = 1/2$, allowing phase slips to occur at a rate that is fast compared to experimental time scales. In our experiments we consider rings to be in thermal equilibrium when no hysteresis is observable in measurements of the ring current vs applied flux. Langer and Ambegaokar's (LA) formula for the phase slip rate provides additional insight for estimating the onset of thermal equilibrium in our rings. LA theory predicts a phase slip rate Γ that depends exponentially on the temperature and the saddle point energy barrier⁸ $\Delta F_{s\pm 1,0}$, Eq. (7):

$$\Gamma \propto \exp\left(-\frac{\Delta F_{s\pm 1,0}(T, \phi)}{k_B T}\right). \quad (8)$$

LA theory is valid only in the limit where $\Delta F_{s\pm 1,0} \gg k_B T$ and phase slips are rare events. We will not make precise predictions for the onset of thermal equilibrium, because the condition for equilibrium, $\Delta F_{s\pm 1,0}(T, \phi) \rightarrow k_B T$, occurs outside the limits of the model. Instead we focus on how the exponential dependence of the phase slip rate affects phase slips in our rings.

At low temperatures phase slips can still occur, but the exponential decrease of the phase slip rate with temperature makes it highly unlikely to encounter phase slips within the measurement time. As a result, when we record the current vs applied flux in our rings at different temperatures, we expect to see no phase slips at the lowest temperatures as long as the applied flux remains low. The flux dependence of $\Delta F_{s\pm 1,0}(T, \phi)$ shows that we could drive phase slips in rings even at the lowest temperatures by applying a larger flux. As the temperature increases we expect the phase slip rate to increase exponentially and eventually become fast compared to the measurement time, bringing our rings into thermal equilibrium.

The following sections explore the effects of fluctuations on the ring's response in thermal equilibrium. Each of the models presented below includes a different set of fluctuations. By comparing the model predictions for different ring parameters we can pinpoint the effect of different fluctuations on ring response and set a physical regime where each type of fluctuations will dominate. Specifically we find that in rings with weak phase stiffness a model including only fluxoid fluctuations accurately reproduces the ring response.

C. Fluxoid number distribution model

We start with a model derived from 1D GL expressions that includes only fluxoid fluctuations. In this model all variation around the ring is described by a single homogeneous phase winding number n . This model is not complete because it does not include local variations in the amplitude or phase. Put another way, this model includes only the large fluctuations between local minima in the GL free energy (see Fig. 1), and ignores all the small fluctuations about each local minimum as well as the saddle points and intermediate states. It is instructive to develop this model because comparisons between this fluxoid-only model and more complete models shed light on what portion of the fluctuation response of a ring is due to solely to fluxoid fluctuations.

We return to the mean-field 1D GL free energy, Eq. (2), which is related to the ring current by $I = -\partial F/\partial \Phi_a$. Taking a derivative yields an expression for the ring current of the n -fluxoid state:

$$I_n(T, \phi) = I^0(T)(\phi - n) \left(1 - \frac{\xi(T)^2}{R^2}(\phi - n)^2\right), \quad (9)$$

where

$$I^0(T) = \frac{2VB_c(T)^2\xi(T)^2}{\Phi_0\mu_0 R^2}. \quad (10)$$

$I^0(T)(\phi - n)$ is the Meissner response, which decreases linearly with increasing temperature close to T_c . The cubic term arises from pair breaking.

The energy associated with each fluxoid current state, $F_n(T, \phi)$, was given in Eq. (2). If phase slips occur at a high enough rate, so that the metastable fluxoid states are in thermal equilibrium as discussed in the previous section, we can model^{4,33} the resulting current response as a Boltzmann distribution of fluxoid states:

$$I_F(T, \phi) = \frac{\sum_n I_n(T, \phi) \exp[-F_n(T, \phi)/k_B T]}{\sum_n \exp[-F_n(T, \phi)/k_B T]}. \quad (11)$$

We label the total ring current generated by fluxoid states I_F to distinguish it from the total ring current including all fluctuation states presented in the next section. We study the susceptibility response of the ring at zero applied flux, $dI(T)/d\phi|_{\phi=0}$. In our rings $L \gg \xi$, so we expand $F_n(T, \phi)$ to lowest order in ξ/R to obtain $F_n(T, \phi) \approx I^0(T)\Phi_0/2(\phi - n)^2 - F_c(T)$. Ignoring the pair-breaking term in the current response yields $I_n(T, \phi) \approx I^0(T)(\phi - n)$. We use these expressions to find the derivative of the total ring current at $\phi = 0$:

$$\frac{dI_F(T)}{d\phi} \Big|_{\phi=0} = I^0(T) \left(1 - \frac{\sum_n 2\sigma n^2 \exp(-\sigma n^2)}{\sum_n \exp(-\sigma n^2)}\right), \quad (12)$$

where $\sigma \equiv I^0(T)\Phi_0/2k_B T$. Equation (12) shows that including a distribution of fluxoid states reduces the ring's susceptibility response from the mean-field value $I^0(T)$. The second term in Eq. (12) is proportional to the rms fluctuation of the fluxoid number n . The magnitude of the reduction in susceptibility depends on σ . When σ is large, terms with $n \neq 0$ are small and the susceptibility is approximately equal to the mean-field value. When σ is small, the $n = \pm 1$ terms begin

to play a significant role. We define a criterion¹ when fluxoid fluctuations reduce the Meissner response by more than 5%:

$$\frac{dI_F(T)}{d\phi} \approx I^0(T) < \frac{12k_B T}{\Phi_0}. \quad (13)$$

In plots of the susceptibility vs temperature we observed a suppression below the mean-field value for susceptibilities below this cutoff. This downturn in the susceptibility signal, which occurs at T less than T_c , is a hallmark of the suppression of the diamagnetic response by fluxoid fluctuations.

D. von Oppen and Riedel model

Thus far, we have considered a fluxoid model that predicts the existence of the downturn in susceptibility below T_c . In some rings, near $T = T_c$, the $L \gg \xi(T)$ assumption we made to obtain Eq. (12) is not valid because L is of order ξ . As a result, the energy between successive metastable states can no longer be approximated by expanding Eq. (2) to lowest order in ξ/R . When we include the quartic term from Eq. (2), the GL free energy vanishes rather than increasing indefinitely for $\phi - n > L/\xi(T)$. Thus, the Boltzmann distribution, Eq. (11), is not well defined because summing over all n leads to a divergent denominator. The numerator on the other hand remains finite since states with $\phi - n > L/\xi(T)$ do not contribute. Furthermore, our treatment thus far has ignored phase fluctuations that are not uniform around the ring and all amplitude fluctuations.

To address these issues, we compare our simple fluxoid model to complete 1D GL theory as formulated by von Oppen and Riedel,³¹ which generates numerical solutions for the susceptibility that include all thermal fluctuations within the GL framework in homogeneous rings. Applying a harmonic oscillator approximation to the VOR model, as discussed in the next section, provides a direct mathematical connection between the VOR model and the fluxoid model discussed in the previous section.

Following von Oppen and Riedel,³¹ we begin with the expression for the GL energy functional given in Sec. II, Eq. (1). In cylindrical coordinates (r, θ, z) , we map the free energy onto a one-dimensional ring geometry with no lateral variation of the order parameter. $\psi(r, \theta, z) = \psi(\theta)$ and $dx^3 = w dR d\theta$. We redefine $R d\theta$ as dx .

We rewrite Eq. (1) using reduced variables $\psi(x) = \bar{\psi}(\bar{x})\sqrt{|\alpha|/\beta}$, $\bar{\nabla} = \xi\nabla$, and $\bar{x} = x/\xi$. $\xi(T)$ is the superconducting coherence length and is given by $\xi(T) = \hbar/\sqrt{2m^*\alpha}$:

$$F[\bar{\psi}(\bar{x})] = E_0(T)k_B T \int_{-\Lambda(T)/2}^{\Lambda(T)/2} \left[\eta |\bar{\psi}(\bar{x})|^2 + \frac{1}{2} |\bar{\psi}(\bar{x})|^4 + \left| \left(\bar{\nabla} - \frac{2\pi i}{\Lambda(T)} \phi \right) \bar{\psi}(\bar{x}) \right|^2 \right] d\bar{x}. \quad (14)$$

η is +1 (−1) for temperatures above (below) the superconducting critical temperature T_c . $\Lambda(T)$ is the reduced circumference $\Lambda(T) = L/\xi(T) = \sqrt{8\pi k_B |T - T_c|/E_c}$ and $E_0(T)k_B T = wd\xi(T)B_c(T)^2/\mu_0$ is the condensation energy of a ring section of length $\xi(T)$. The correlation energy for the ring, $E_c = \pi^2 \hbar v_f \ell_e / 3L^2$, includes the mean free path ℓ_e and

the Fermi velocity v_f , which is 2.03×10^6 m/s in aluminum. $E_0(T)$ can also be written as

$$E_0(T) = \frac{(2\pi)^{5/2}}{21\zeta(3)} \left(\frac{k_B |T - T_c|}{E_c} \right)^{3/2} \frac{E_c M_{\text{eff}}}{k_B T}, \quad (15)$$

where $\zeta(3) = 1.021$ is the Riemann zeta function. $M = k_f^2 wd/4\pi$ is the number of transverse channels. k_f is the Fermi wave vector, which for an aluminum ring is $k_f = 1.75 \times 10^{10}$ m^{−1}. Including disorder results in an effective number of channels $M_{\text{eff}} = M \ell_e / L$.

We obtain the thermodynamic expression of the current from the flux derivative of the ring's partition function,

$$I(T, \phi) = -k_B T \frac{1}{Z_{sc}} \frac{\partial}{\partial \Phi_a} Z_{sc}. \quad (16)$$

The partition function is the path integral of the GL free energy,

$$Z_{sc} = \int [d\bar{\psi}(\bar{x})][d\bar{\psi}^*(\bar{x})] \exp \left(\frac{-F[\bar{\psi}(\bar{x})]}{k_B T} \right). \quad (17)$$

The VOR model uses a transfer matrix technique³⁶ to map the Ginzburg-Landau path integral partition function, Eq. (17), onto another partition function

$$Z = \sum_{l=-\infty}^{\infty} \exp(-i2\pi l\phi) \sum_{n=0}^{\infty} \exp[-2E_0(T)\Lambda(T)\mathcal{E}_{n,l}], \quad (18)$$

where $\mathcal{E}_{n,l}$ are the eigenvalues of the fictitious 2D single-particle Hamiltonian

$$H = -\frac{1}{8E_0(T)^2} \nabla^2 + \frac{1}{2} \eta \vec{r}^2 + \frac{1}{4} \vec{r}^4. \quad (19)$$

We define $\vec{\rho} = [2E_0(T)]^{1/3} \vec{r}$ and rewrite Eqs. (18) and (19) to emphasize the parameter $\gamma(T)$:²

$$Z = \sum_{l=-\infty}^{\infty} \exp(-i2\pi l\phi) \sum_{n=0}^{\infty} \exp[-\gamma(T)^{1/3} \mathcal{E}_{n,l}], \quad (20)$$

$$H = -\frac{1}{2} \nabla^2 + \frac{1}{2} \frac{\Lambda(T)^2}{\gamma(T)^{2/3}} \vec{\rho}^2 + \frac{1}{4} \vec{\rho}^4. \quad (21)$$

The temperature dependence is set by the coherence length through the relation $\Lambda(T) = L/\xi(T)$. The parameter

$$\gamma(T) \equiv \frac{\Lambda(T)^3}{2E_0(T)} = \frac{42\zeta(3)}{\pi} \frac{k_B T}{M_{\text{eff}} E_c} \quad (22)$$

determines the relative effect of fluxoid fluctuations on the ring's susceptibility response.² γ is related to the physical ring parameters as $\gamma \propto TL^3/wd\ell_e^2$. The $\gamma(T)$ parameter is also inversely proportional to the superconducting phase stiffness K , which we express in terms of our parameters as $K = L\Lambda(T)^2/w\gamma(T)$.³⁷ For rings with larger $\gamma(T)$, as the temperature approaches T_c several phase winding states are thermally accessible and contribute to suppression of the susceptibility. The definition of γ introduced by Koshnick *et al.*² made the approximation $T = T_c$. The larger temperature range explored in this paper makes it necessary to reintroduce the T dependence. We use the relation $I^0(T) = 4\pi^2 k_B T L^2 / \Phi_0 \xi(T)^2 \gamma(T)$ to compare the VOR model to the mean-field and fluxoid models.

Equations (20) and (21) can be solved numerically. The Hamiltonian can be rewritten as a harmonic oscillator with

a quartic perturbation. We write matrix elements in terms of the coefficients and diagonalize numerically to find the eigenvalues.^{35,38} The eigenvalues are used in the partition function, Eq. (20), and substituted into the thermodynamic equation for the current, Eq. (16), to generate the full current response. We find the zero-field susceptibility by taking a derivative with respect to applied flux at $\phi = 0$.

Analytical solutions can be instructive, and as a result it is useful to find approximations to the full VOR model that are valid over some set of ring parameters or temperatures. One such approximation is to ignore the quartic perturbation to the Hamiltonian, which then takes the form of a simple harmonic oscillator. Moreover, making this approximation provides a direct mathematical connection between our fluxoid model and the full 1D GL model of VOR.

E. Harmonic oscillator model

The harmonic oscillator (HO) approximation is valid at temperatures well below T_c , where the wave functions contributing to Eq. (20) extend over only a narrow region around the minimum of the Mexican hat potential of Eq. (21), so that the latter can be approximated by a quadratic expansion. In this case, fluctuations from the quartic nature of the potential should not play a significant role. We refer to the fluctuations in this model as quadratic fluctuations, rather than Gaussian fluctuations, to avoid confusion with small order parameter fluctuations above T_c , which are often referred to as Gaussian fluctuations.

We can quantify the range of validity for the HO model using the Ginzburg parameter. The Ginzburg parameter is $G_i = |T_{LG} - T_c|/T_c$, where T_{LG} is the temperature where the heat capacity due to fluctuations is equal to the heat capacity jump at the critical temperature. We can rewrite the Ginzburg parameter with respect to $\gamma(T)$, $T_c/E_c G_i \propto \sqrt{\gamma}$.² At temperatures below the limit set by the Ginzburg parameter, fluctuations are small and approximated as quadratic fluctuations from GL theory, and the HO model is valid. At temperatures close to T_c , the quartic term becomes significant and a nonperturbative approach, presented in the previous section, is required to capture the fluctuation response.

Eigenstates of the Hamiltonian given in Eq. (21) have the form $\vec{r} = |r| \exp(i\ell\phi)$, so the Hamiltonian can be written as a 1D problem, $H = -\frac{1}{2} \frac{d^2}{dr^2} + V(r)$, where

$$V(r) = \frac{l^2}{2r^2} + \frac{1}{2} \frac{\Lambda(T)^2}{\gamma(T)^{2/3}} r^2 + \frac{1}{4} r^4. \quad (23)$$

Expanding $V(r)$ about its minimum at $R_m(l)$ leads to the eigenvalues

$$\mathcal{E}_{n,l} = \frac{l^2}{2R_m(l)^2} + \frac{R_m(l)^4}{4} + \omega(n + 1/2), \quad (24)$$

where $\omega = \sqrt{\Lambda(T)^2/\gamma(T)^{2/3} + 3R_m(l)^2 + 3l^2/R_m(l)^4}$.

Only terms that change with l , the angular momentum coordinate in the fictitious Hamiltonian, contribute to the flux dependence of the partition function; thus only these terms contribute to the thermodynamic ring current. If we make an approximation and only include the $l^2/2R_m(l)^2$ terms, where

$R_m(0)$ is the value for r that minimizes $V(r)$ when $l = 0$, the current from Eq. (16) is

$$I_{HO}(T, \phi) = \frac{k_B T}{\Phi_0} \frac{\sum_{l=1}^{\infty} 4\pi l \sin(2\pi l\phi) \exp[l^2\gamma(T)/2\Lambda(T)^2]}{1 + \sum_{l=1}^{\infty} 2 \cos(2\pi l\phi) \exp[l^2\gamma(T)/2\Lambda(T)^2]}, \quad (25)$$

which is exactly equivalent the fluxoid current Eq. (11). Through this approximation we are able to show a direct link between the harmonic oscillator approximation to the VOR model and the fluxoid model. Including the second two terms of Eq. (24), which account for the angular momentum dependence of ω and $R_m(l)$, we get

$$Z = \sum_{l=-\infty}^{\infty} \exp(-i2\pi l\phi) \exp[-\gamma(T)^{1/3} V(R_m(l))] \times \frac{\exp[-\gamma(T)^{1/3}\omega/2]}{1 - \exp[-\gamma(T)^{1/3}\omega]}. \quad (26)$$

Using this simplified partition function we can find the ring's current and consequently its susceptibility in the limit where we ignore only quartic fluctuations.

F. Comparison of models

We have presented the theoretical basis for four models including the mean-field model, the fluxoid model, the harmonic oscillator model, and complete 1D GL theory as formulated by von Oppen and Riedel. We now compare the physics captured by each model in Fig. 2 by plotting the theoretical susceptibility response as a function of temperature for rings with three different $\gamma(T = T_c)$ parameters.

The mean-field model is our baseline. It gives the ring response in the absence of all superconducting fluctuations. At the other extreme, the VOR model incorporates all thermally activated GL fluctuations into the ring response. In between we have the fluxoid model, which includes only fluxoid fluctuations, and the harmonic oscillator model which ignores only quartic fluctuations. By comparing these models for rings with different $\gamma(T = T_c)$ we determine how fluctuations contribute to the response.

One striking feature in all three Fig. 2 plots is that both the VOR model and its HO approximation have an offset in the linear regime, far below T_c , compared to the mean-field and fluxoid models. This downshift reflects a renormalization in T_c due to consideration of all possible fluctuation modes.

Figure 2(a) shows a ring with $\gamma(T = T_c) = 3$. The low γ parameter means it has strong phase stiffness, making fluxoid fluctuations unlikely. The temperature range where we expect to encounter fluctuations is very close to T_c . The two models that include only quadratic fluctuations, the HO model and the fluxoid model, both fail to reproduce the line shape of the VOR model for this ring. We are clearly within the temperature range prescribed by the Ginzburg parameter where quartic fluctuations must be taken into account. Susceptibility-enhancing amplitude fluctuations at and above T_c overwhelm the susceptibility reduction expected from fluxoid fluctuations. A downturn is not observable;

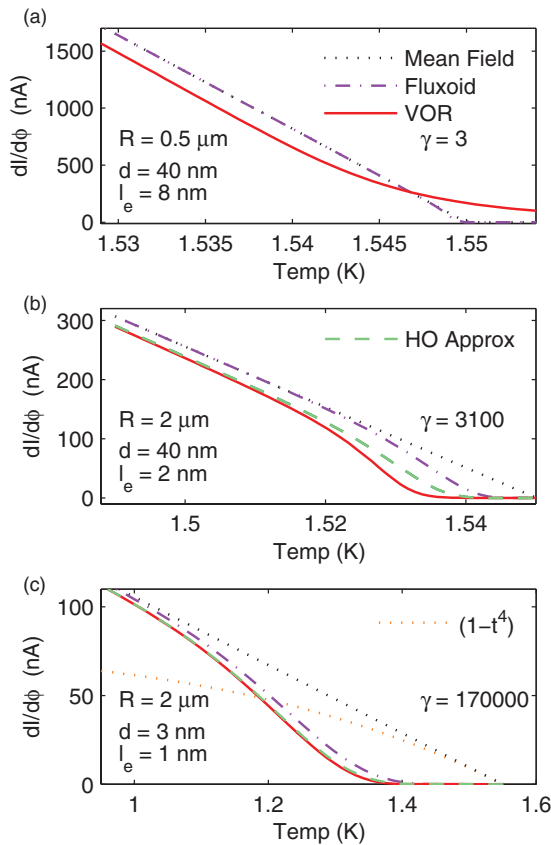


FIG. 2. (Color online) Theoretical susceptibilities calculated using the mean-field model, black dotted line, Eq. (10); the fluxoid model, purple dot-dashed line, Eq. (12); the VOR model, red solid line, Eqs. (16), (20), and (21); and its approximate HO solution, green dashed line, Eqs. (16) and (26), for rings with $w = 80$ nm and $T_c = 1.55$ K. For all values of $\gamma(T = T_c)$, the VOR and HO response well below T_c match the mean-field and fluxoid predictions only if T_c is renormalized. (a) $\gamma(T = T_c) = 3$. The VOR model predicts a susceptibility above T_c . (b) $\gamma(T = T_c) = 3100$. A downturn occurs at $dI/d\Phi \approx 12k_B T/\Phi_0 \approx 120$ nA, $T \approx 1.52$ K. The fluxoid, HO, and VOR models reproduce the overall line shape of the downturn, up to an offset in T_c . However, the three models predict downturns of different sizes, with the largest predicted by the VOR model. (c) $\gamma(T = T_c) = 170000$. Fluxoid fluctuations dominate the response over a wide temperature range and the fluxoid and HO models become increasingly accurate predictors of the full fluctuation theory. The orange dotted line added to (c) is the $(1 - t^4)$ temperature dependence which limits the validity of GL theory.

instead the small $\gamma(T = T_c)$ leads to a susceptibility signal above T_c .

When $\gamma(T = T_c) = 3100$, as shown in Fig. 2(b), the fluxoid-induced downturn becomes visible below T_c , starting at $T \approx 1.52$ K and 120 nA, as predicted by our fluxoid criterion, Eq. (13). All three fluctuation models qualitatively reproduce the shape of the susceptibility suppression. As expected, the VOR model predicts a greater susceptibility suppression than the fluxoid or HO model, because only the VOR model includes all thermal fluctuations. The excess suppression between the fluxoid and VOR models is presumably due to contributions from nonhomogeneous phase winding solutions, amplitude fluctuations, or both, while the excess

suppression between the HO and VOR models is due to fluctuations caused by the quartic nature of the potential.

For $\gamma(T = T_c) = 170000$, shown in Fig. 2(c), the susceptibility response is dominated by fluxoid fluctuations, shown by the almost identical line shape shared by the fluxoid model and the VOR model. The total response is also well represented by the harmonic oscillator approximation, showing that in this region nearly all fluctuations are quadratic in nature.

Figure 2(c) shows a larger temperature range than the previous panels, and the GL approximation that T is close to T_c is not valid over the whole plot. GL theory is valid in the range of temperature where the linear mean-field response approximates a temperature dependence that varies as $(1 - t^4)$, $t = T/T_c$, shown as an orange dotted line. An alternative criterion is that $T > \Delta(T)$, where $\Delta(T)$ is the superconducting gap. These both result in approximately the same range of validity. GL theory has been applied with success at temperatures far from T_c , but interpretation of results in this regime should be treated with caution. The $(1 - t^4)$ dependence is not included in Figs. 2(a) and 2(b) because all plotted temperatures lie within the valid range.

In the next section we describe our measurement of ring susceptibility for rings with different $\gamma(T = T_c)$. We find good agreement between our data and the fluctuation response predicted by the fluxoid model and full 1D GL theory.

III. SAMPLE AND MEASUREMENT TECHNIQUE

A. Sample preparation

We measured quasi-one-dimensional superconducting rings in a dilution refrigerator³⁹ with a scanning SQUID susceptometer⁴⁰ that was specifically designed for this purpose. We focus on data from two different samples expected to exhibit fluxoid fluctuations. Sample I's rings were fabricated and measured previously.³³ The rings were narrow and dirty with $T_{c1} \approx 1.5$ K. They were made by depositing a 40-nm-thick aluminum film by *e*-beam evaporation at a rate of about 1 Å/s and a pressure of approximately 10^{-6} mbars on a Si substrate patterned with poly(methyl methacrylate) (PMMA) resist. During the deposition, the rate temporarily dropped to a negligible level for about 10 min and subsequently recovered. This unintentional delay caused the formation of two superconducting layers separated by an AlO_x tunneling barrier. The coupling between the two Al layers depended on the width of the rings, with narrow rings ($w \leq 190$ nm) and wide rings ($w \geq 250$ nm) showing a single order parameter. Intermediate widths showed evidence of weak interactions between the two layers, leading to two-order-parameter effects.³³ In this work we only present data from the narrow rings which showed no two-order-parameter behavior. However, due to the oxidation process we suspect that the thinnest rings have a large oxidized layer that reduces the thickness of the superconductor. Consequently we expect that these rings have an effective height that is less than 40 nm. We can test this prediction by extracting the ring's cross section from fits to the VOR model.

The rings on sample II were fabricated specifically for this paper. The fabrication process was almost identical to the rings from sample I except the evaporated film was thinner,

$d = 15$ nm, and there was no interruption in the evaporation. The deposited rings were wide and dirty with $T_{cII} \approx 2.1$ K. Of the many fabricated rings of different widths and radii, only the widest rings, $w \approx 850$ nm, had a diamagnetic response. The next widest rings, $w \approx 450$ nm, showed no signs of superconductivity indicating that they were oxidized throughout. This evidence makes it difficult to predict with certainty what portion, if any, of the 850 nm rings are oxidized. For each sample we used Ginzburg-Landau models^{3,33,41} to fit a zero-temperature penetration depth $\lambda_I(0) \approx 800$ nm, $\lambda_{II}(0) \approx 1.5$ μm and coherence length $\xi_I(0) \approx 80$ nm, $\xi_{II}(0) \approx 30$ nm.

The agreement with theory is perhaps surprising given that our rings may not be in the 1D limit. We note that finding agreement between the data and the model is not sufficient to prove the correctness of the theory. Zhang applied finite-width corrections to 1D GL theory and found close agreement in the susceptibility response of 1D and 2D rings.³⁵ Despite the large width of the rings, Abrikosov vortices are not expected to be present in our rings at low applied fields^{12,21} and thus will not impact our zero-field susceptibility measurements.

B. Measurement

Measurements were done with a voltage-biased dc SQUID susceptometer amplified by a series-array SQUID preamplifier.⁴² The SQUID is mounted on a piezoresistive scanning assembly,³⁹ which is connected to the mixing chamber of a dilution refrigerator through a single copper braid. The temperature of the scanner and sample is controlled with submillikelvin precision through feedback. The SQUID sensor's counterwound geometry, with on-sensor modulation coils for feedback, enables cancellation of an applied field to one part in 10^4 .⁴⁰ The ring current is measured by positioning the SQUID about 1 μm above the ring and recording the flux induced by the ring's current in the SQUID's 4.6 μm diameter pickup loop. During the measurement, the applied flux threading the ring is varied by several flux quanta at a few hertz by an on-sensor field coil. This measurement is repeated 13 μm above the ring, and the ring signal is computed as the difference between the two positions for each value of applied flux. This procedure allows us to achieve an additional three orders of magnitude of background cancellation. A more detailed description of the measurement system was given by Koshnick *et al.*²

We plot the flux induced in the SQUID's pickup loop as a function of the flux applied by the field coil in Fig. 3 for two different rings. The measurement is repeated to record the full temperature dependence of the ring's response. The ring current I is coupled as flux into the SQUID pickup loop through their mutual inductance M . $\Phi_{\text{SQUID}} = MI$. We estimate the mutual inductance between the SQUID pickup loop and a ring by calculating the mutual inductance between two on-axis rings with radii r_1 and r_2 a distance z apart:

$$M = \pi \mu_0 r_1 r_2 \int_0^\infty dk e^{-\kappa|z|} J_1(\kappa r_1) J_1(\kappa r_2). \quad (27)$$

J_1 is a Bessel function of the first kind. For all our mutual inductance calculations we assume a ring–pickup loop separation of 1 μm . Through a separate fitting technique³³ we

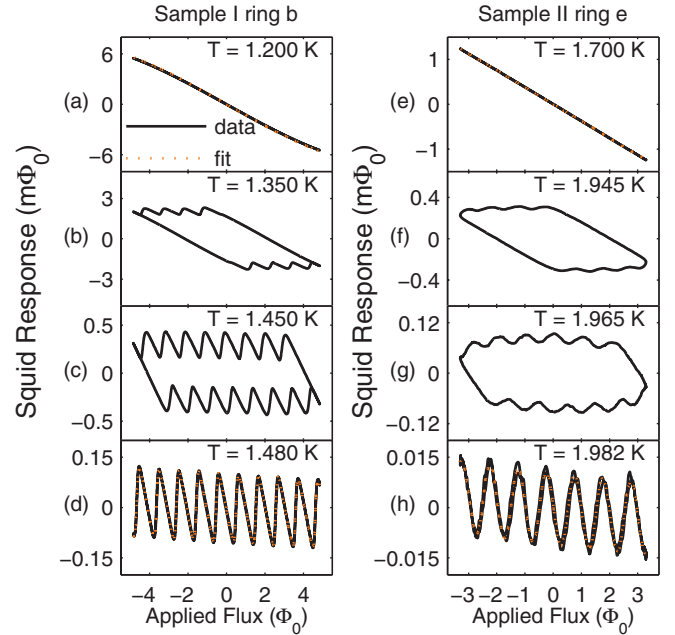


FIG. 3. (Color online) Plots of SQUID response vs applied flux at different temperatures for a ring from each of the two samples. Rings (b) and (e) refer to specific rings plotted in Fig. 4. Ring (b) $T_c = 1.56$ K and ring (e) $T_c = 2.08$ K. The curves evolve from nonhysteretic with no fluxoids at low temperatures, through a hysteretic regime, to nonhysteretic with a change in fluxoid number at every applied flux quantum near T_c . The orange dotted lines are fits to the GL current, Eq. (9), at low temperatures and to the Boltzmann distribution, Eq. (11), at high temperatures. We extract the ring's susceptibility at each temperature by taking the derivative at $\phi = 0$.

estimate the actual distance between the pickup loop and the ring to range from 0.75 to 1.1 μm . Ring currents and susceptibilities quoted later in this paper have error bars that reflect this systematic uncertainty in the coupling factor, which would shift the entire data set.

The ring response curves plotted in Fig. 3 evolve from cubic and nonhysteretic at low temperatures through a hysteretic regime to periodic and nonhysteretic near T_c . At low temperatures the current response is well described by the GL current with no phase windings, Eq. (9) with $n = 0$, shown as an orange dotted line in Figs. 3(a) and 3(e). Due to the low temperatures and small applied flux the energy barrier for phase slips is large compared to $k_B T$. As a result, no phase slips occur on the scale of the measurement time and the ring remains in the $n = 0$ fluxoid state. As the temperature increases and approaches the saddle point energy barrier, phase slips begin to occur, which allows the ring to transition to higher fluxoid states; however, the phase slip rate is still slow compared to the measurement time leading to a hysteretic response.

Finally, as the temperature approaches T_c , the phase slip rate becomes fast and the ring relaxes to thermal equilibrium. As the flux is swept, phase winding transitions occur within some range of $\phi = n + 1/2$. The ring's response is no longer hysteretic and can be modeled as a Boltzmann distribution of all fluxoid states, Eq. (11), shown as an orange dotted line in Figs. 3(d) and 3(h). We extract the magnetic susceptibility

of the ring at each temperature where the ring is in thermal equilibrium by fitting a low-order polynomial to obtain the slope at $\phi = 0$.

C. Susceptibility data

We measured 38 rings on sample I and 12 rings on sample II. Sample I was fabricated and measured primarily for a different experiment.³³ As a result, only eight of the rings measured have sufficient susceptibility data over a wide enough temperature range to make comparisons with the models presented in the previous section. Two representative rings were selected from sample I for this paper. The three rings from sample II were chosen to show a variety of ring parameters and because they had the densest susceptibility data over the important temperature range. The set of five rings allows us to explore the effects of ring size and mean free path on the fluctuation response. Figure 4 shows the susceptibility vs temperature data for the five rings. Each ring's physical parameters are given in Table I. We extracted the ring radii from the flux periodicity of the ring's response in thermal equilibrium and confirmed the measurement through scanning electron microscope (SEM) imaging. The ring thicknesses were measured with atomic force microscopy (AFM), and the width with SEM. Fitting to the VOR model allowed us to estimate values for the ring's cross section and mean free path. We used the measured ring width and thickness plus an additional error factor as an upper limit on the cross-section parameter in the VOR model for rings (c)–(e). No lower limit was enforced due to the possibility that oxidation may have reduced the superconducting cross section.

Figure 4 plots the susceptibility vs temperature curves for five rings. The blue susceptibility data points represent the slope at $\phi = 0$ of the SQUID response at different temperatures scaled by the ring-SQUID mutual inductance to obtain the ring current. The error bars represent height errors in our calculation of the mutual inductance, Eq. (27). This error is systematic and expected to be the same for all points in a panel. Using T_c , and the temperature independent portions of $\gamma(T)$ and $E_0(T)$ as the free parameters, the red line is a fit of the data to the VOR model, Eqs. (16), (20), and (21). The fit results used to generate the red curves are given in Table II. We report values for $\gamma(T)$ at T_c and $E_0(T)$ at $T = 0$. The reported T_c represents the nominal mean field T_c entering the VOR model.³¹ The fitted values of $\gamma(T = T_c)$ are also listed on each of the plots. The black dotted line is the mean-field ring response, Eq. (10), which is the expected response if no fluctuations are present. Deviations in the data from the black dotted line show the influence of fluctuations on a given ring. Finally, the gray region of the curve is the 95% confidence interval obtained from bootstrapping.

Using the fit results from Table II along with the known values of the ring radii given in Table I, we can extract values for the ring's cross section and mean free path from the expressions for $E_0(T)$, Eq. (15), and $\gamma(T)$, Eq. (22). The ring parameters obtained in this way are given along with their 95% confidence intervals in Table I. We note that the mean free paths extracted from VOR fits for rings (c)–(e) are extremely small, $\ell_e \sim 1 \text{ \AA}$. Physically the mean free path is the distance electrons travel before scattering, which should be limited to

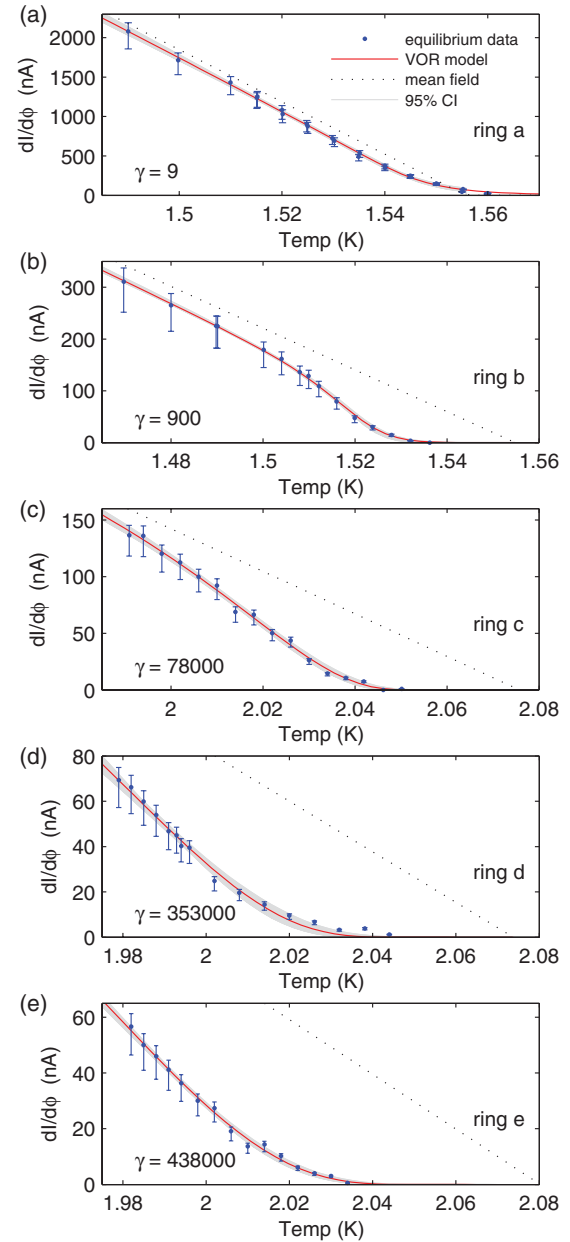


FIG. 4. (Color online) Zero-field susceptibility (blue dots) vs temperature plotted for five different rings. In all plots the solid red line is a fit to the VOR model, Eqs. (16), (20), and (21). The dotted black line is the expected mean-field susceptibility given by $I^0(T)$, Eq. (10), using the VOR fit parameters. The gray-shaded area represents the 95% confidence interval from bootstrapping. The error bars represent the systematic uncertainty in the SQUID-ring mutual inductance.

the lattice constant of 4 \AA in aluminum. However, as a fit parameter these low values are consistent with mean free paths extracted from measurements of H_{eff} in thin aluminum films.⁴³ Alternatively these small mean free paths may indicate that we are reaching the limits of the validity of 1D GL theory for rings with especially large widths or that the fit is underconstrained as described below.

Due to the evaporation conditions discussed previously, we are not confident that the entire cross section of each ring is

TABLE I. Table of ring values. Values for the cross section and mean free path, extracted from fits to the VOR model, are given with their 95% confidence interval (CI). An upper limit of $14\,790\text{ nm}^2$ was enforced on the ring cross section to constrain the fits for rings (c)–(e).

Ring	Directly measured			Extracted from VOR fits			
	R (μm)	w (nm)	d (nm)	wd (nm^2)	95% CI	ℓ_e (nm)	95% CI
(a) (I)	0.50	123	40	1598	1140–2314	6.4	4.3–9.4
(b) (I)	1.97	90	40	583	492–1177	8.5	4.4–10.4
(c) (II)	1.21	840	15	13319	2811–14790	0.11	0.09–0.48
(d) (II)	1.75	850	15	14790	11896–14790	0.08	0.07–0.11
(e) (II)	1.82	850	15	13602	9172–14790	0.08	0.07–0.12

superconducting. For the two rings on sample I the fitted cross sections are smaller than the values found using AFM and SEM, which confirms our suspicion that a portion of the ring is oxidized. The data from the three sample II rings are within the downturn region, i.e., the decrease in the susceptibility is not linear even at the lowest plotted temperatures. In practice, we are limited on the low end of the temperature range by the point where the SQUID response curves become hysteretic. A three-parameter fit is underconstrained, and it is consequently difficult to get accurate VOR fits without susceptibility data at lower temperatures, including the point where the data are reduced from the linear response. As a result, for rings (c)–(e) we put a strict upper limit of $wd = 14\,790\text{ nm}$ on the cross section, which acted as an additional constraint on the VOR fits. The cross sections extracted from fits to the constrained VOR model for the rings on sample II agree well with the AFM-SEM cross section indicating little oxidation. A similar limit was not applied to rings (a) and (b) because data in the linear susceptibility region kept the fit from being underconstrained. We find good agreement between the susceptibility data and fits to the VOR model for all rings except ring (d), where it is clear that the VOR model does not capture the shape of the data at high temperatures. It is unclear why the VOR model provides a poor fit for this ring. It is possible that errors from extracting the susceptibility near T_c , errors that are not accounted for in the error bars, are particularly large for measurements on this ring.

Looking at the sequence of five rings it is clear that the extent of the suppression of superconductivity increases as $\gamma(T = T_c)$ increases. This is just what we expect for a series of rings where fluxoid fluctuations play a larger and larger role.

Ring (a) shows an enhancement of the superconducting response above T_c . This response is caused by amplitude

fluctuations and has been studied by Koshnick *et al.*² and Zhang and Price.³ As we showed in our description of the theoretical models, only the VOR model can correctly reproduce the upturn in susceptibility above T_c .

The remaining four rings in Fig. 4 show a suppression of the susceptibility signal below the mean-field response (black dotted line). However, of the plotted rings only ring (b) has a large enough temperature range to observe a downturn from the linear regime. The downturn for ring (b) occurs at $T \approx 1.52\text{ K}$ and 120 nA , which corresponds to the criterion for fluxoid fluctuations given in Eq. (13). Such agreement validates our criterion for the onset of susceptibility suppression driven by fluxoid fluctuations. The free energy configuration space for ring (b) resembles Fig. 1(a) where phase slips onset and bring the ring into thermal equilibrium before fluxoid fluctuations at zero applied flux are energetically accessible. The full temperature range plotted for rings (c)–(e) is already deep in the suppression region. This is due to the fact that for rings (c)–(e) fluxoid fluctuations and phase slips onset at approximately the same temperature as shown in Fig. 1(b). In the next section we expand the temperature range by adding susceptibility data from lower-temperature hysteretic ring response curves. The additional data confirm that the response is suppressed from the mean-field value.

We have shown that the VOR model, based on 1D GL theory, describes the temperature dependence of the susceptibility. To get a feeling for the type of fluctuations that play a role in the ring response we plot the fluxoid model and the HO model in addition to the VOR model and mean-field model for ring (c) in Fig. 5. It is clear that fluxoid fluctuations cause the majority of the suppression. Quadratic fluctuations of a nonfluxoid nature described by the HO model contribute to

TABLE II. Table of fitted values. We used the temperature-independent portions of $\gamma(T)$ and $E_0(T)$ as fit parameters in the VOR model. This table reports values for $\gamma(T = T_c)$ and $E_0(T = 0)$ as well as the limits of the 95% confidence interval (CI) obtained from bootstrap analysis for the data presented in Fig. 4.

Ring	T_c (K)	95% CI	$\gamma(T = T_c)$	95% CI	$E_0(T = 0)$	95% CI
(a) (I)	1.556	1.554–1.557	9.20	6–14	2138	1850–2550
(b) (I)	1.555	1.550–1.556	899	760–1660	898	820–1300
(c) (II)	2.076	2.072–2.086	78×10^3	$(18\text{--}95) \times 10^3$	2650	1180–2870
(d) (II)	2.074	2.066–2.083	353×10^3	$(261\text{--}443) \times 10^3$	2590	2280–2730
(e) (II)	2.080	2.075–2.086	438×10^3	$(294\text{--}536) \times 10^3$	2370	1910–2550

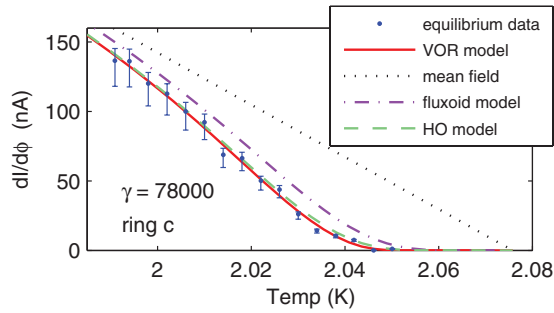


FIG. 5. (Color online) Comparison of the four models plotted using parameters obtained from fitting the data from ring (c) to the VOR model. Fitting to the fluxoid model would yield an equally good fit with a slightly different T_c .

the renormalization of T_c , and quartic fluctuations described by the VOR model play only a minor role. In fact the fluxoid model would fit the data equally well with just a shift in the T_c .

The data set, taken as a whole, confirms the points we made throughout this paper. Fluxoid fluctuations not only suppress the rings' superconducting response but play an increasingly large role in the suppression as $\gamma(T = T_c)$ increases. We showed that our susceptibility vs temperature data are well described by a GL model for homogeneous rings, formatted by von Oppen and Riedel,³¹ that includes all thermally activated fluctuations. The largest- γ rings can be equally well described by our simple fluxoid-only model. Furthermore, we can use fits to the VOR model to reproduce some of the rings' physical parameters including the cross section and mean free path. Finally, by using VOR fit parameters we can employ our two approximate models, the fluxoid model and the harmonic oscillator model, to determine the how much of the suppression is due to either fluxoid fluctuations or quartic fluctuations, shown for ring (c) in Fig. 5.

D. Hysteretic susceptibility data

For rings (c)–(e) in Fig. 4 we expect the onset of the downturn induced by fluxoid fluctuations to occur in a temperature range where the SQUID response curves are hysteretic, as shown in Fig. 3. This is due to the fact that in these longest, dirtiest rings $L \gg \xi(T)$ and fluxoid fluctuations are already energetically favorable at the temperature when phase slips begin to occur, as discussed in Sec. II A. Fluxoid fluctuations are never energetically favorable for ring (a) and they onset well after phase slips in ring (b). From the ring (b) susceptibility data we see that phase slips onset at ~ 1.3 K while fluxoid fluctuations onset at ~ 1.51 K.

To demonstrate that the data presented represent a real reduction in the ring response, we examine the susceptibility signals at lower temperatures that fall in the hysteretic regime. We extract susceptibility data by taking the slope at zero current on the long continuous sides of the hysteretic curves.

Figure 6 shows susceptibility data in the hysteretic regime (green points with error bars) and reproduces the susceptibility data and fits from the nonhysteretic regime (blue points and solid red line) from rings (b)–(e) in Fig. 4. Figure 6 also shows

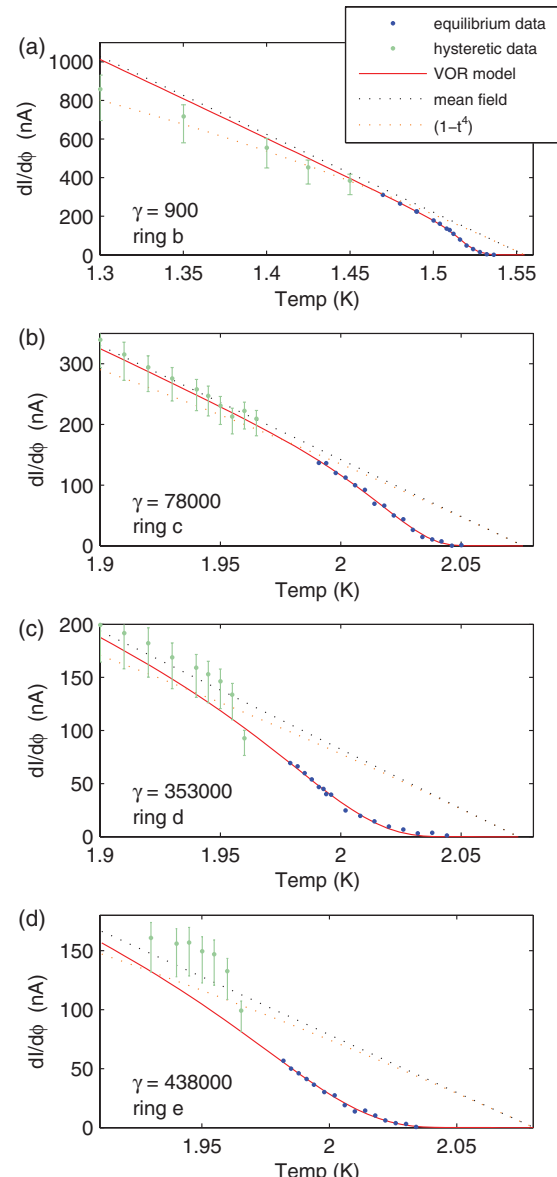


FIG. 6. (Color online) Susceptibility data from rings (b)–(e). The green points with error bars are the slopes of the hysteretic curves, which estimate the susceptibility in the hysteretic regime. The error bars account for a systematic error in the coupling constant that would shift all points together. The blue points are reproduced from Fig. 4, which plots the susceptibility of the ring's response in thermal equilibrium. The red solid line is a fit of the blue nonhysteretic data to the VOR model and the black dotted line is the mean-field response; both are reproduced from Fig. 4. Also plotted is the $(1 - t^4)$ temperature dependence which limits the validity of GL theory.

the $(1 - t^4)$ dependence, plotted as an orange dotted line, that sets the validity of our GL-based models.

The hysteretic data points in rings (c)–(e), Figs. 6(b)–6(d), follow the mean-field curve until a crossover point when they line up with the VOR model and the higher-temperature susceptibility data. This provides evidence that the susceptibility measured from the SQUID response curves in thermal equilibrium is suppressed from the mean-field value. The drop in susceptibility from the mean-

field value occurs when the phase slip rate is sufficiently high and multiple fluxoid states compete to suppress the response.

IV. CONCLUSIONS

Superconducting phase slips in one-dimensional rings and wires have been the subject of theoretical and experimental interest for decades. While phase slips in 1D structures determine the onset of resistance, the fluxoid processes we described here cause the loss of another hallmark of superconductivity, the ability to screen magnetic fields. In this paper we have outlined four models that describe the effects of superconducting fluctuations on the susceptibility response in rings. We have shown that the responses of rings with various physical parameters can be characterized by 1D GL theory as described by von Oppen and Riedel for uniform rings, which includes all thermal fluctuations. By comparing the models we can determine the types of fluctuation that contribute to the response of a given ring. We found that

for rings with weak phase stiffness the ring response can be described using a fluxoid-only model, indicating that these types of fluctuations are the dominant cause of suppression of the susceptibility signal. One could imagine extending this ring system to a weakly connected grid, linking our results to the field of percolation superconductivity. Additionally, achievable experimental conditions allow fluxoid fluctuations to occur at temperatures down to 50 mK. Such a setup could provide experimental conditions for examining the quantum mechanical behavior of a 1D ring.⁴⁴

ACKNOWLEDGMENTS

This work was supported by NSF Grant Nos. DMR-0803974, DMR-0507931, and PHY-0425897 and by the Packard Foundation. Work was performed in part at the Stanford Nanofabrication Facility, which is supported by NSF Grant No. ECS-9731293, its laboratory members, and industrial affiliates. We express gratitude to Martin Huber for assistance in SQUID design and fabrication.

^{*}Present address: Department of Physics, RWTH Aachen University, Aachen Germany.

[†]kmoler@stanford.edu

¹N. C. Koshnick, Ph.D. thesis, Stanford University, 2009.

²N. C. Koshnick, H. Bluhm, M. E. Huber, and K. A. Moler, *Science* **318**, 1440 (2007).

³X. Zhang and J. C. Price, *Phys. Rev. B* **55**, 3128 (1997).

⁴W. Skocpol and M. Tinkham, *Rep. Prog. Phys.* **38**, 1049 (1975).

⁵V. Emery and S. Kivelson, *Nature (London)* **374**, 434 (1995).

⁶J. M. Kosterlitz and D. J. Thouless, *J. Phys. C* **6**, 1181 (1973).

⁷T. M. Rice, *Phys. Rev.* **140**, A1889 (1965).

⁸J. S. Langer and V. Ambegaokar, *Phys. Rev.* **164**, 498 (1967).

⁹D. E. McCumber and B. I. Halperin, *Phys. Rev. B* **1**, 1054 (1970).

¹⁰N. Giordano, *Phys. Rev. Lett.* **61**, 2137 (1988).

¹¹C. N. Lau, N. Markovic, M. Bockrath, A. Bezryadin, and M. Tinkham, *Phys. Rev. Lett.* **87**, 217003 (2001).

¹²B. J. Baelus, F. M. Peeters, and V. A. Schweigert, *Phys. Rev. B* **61**, 9734 (2000).

¹³J. Berger, *Phys. Rev. B* **67**, 014531 (2003).

¹⁴H. Bluhm, N. C. Koshnick, M. E. Huber, and K. A. Moler, e-print arXiv:0709.1175.

¹⁵S. Pedersen, G. R. Kofod, J. C. Hollingsby, C. B. Sørensen, and P. E. Lindelof, *Phys. Rev. B* **64**, 104522 (2001).

¹⁶D. Y. Vodolazov, F. M. Peeters, S. V. Dubonos, and A. K. Geim, *Phys. Rev. B* **67**, 054506 (2003).

¹⁷J. E. Lukens and J. M. Goodkind, *Phys. Rev. Lett.* **20**, 1363 (1968).

¹⁸A. D. Hernández, B. J. Baelus, D. Domínguez, and F. M. Peeters, *Phys. Rev. B* **71**, 214524 (2005).

¹⁹M. Morelle, D. S. Golubović, and V. V. Moshchalkov, *Phys. Rev. B* **70**, 144528 (2004).

²⁰V. Bruyndoncx, L. Van Look, M. Verschueren, and V. V. Moshchalkov, *Phys. Rev. B* **60**, 10468 (1999).

²¹J. R. Kirtley, C. C. Tsuei, V. G. Kogan, J. R. Clem, H. Raffy, and Z. Z. Li, *Phys. Rev. B* **68**, 214505 (2003).

²²J. Berger and J. Rubinstein, *Phys. Rev. B* **56**, 5124 (1997).

²³L. D. Jackel, W. W. Webb, J. E. Lukens, and S. S. Pei, *Phys. Rev. B* **9**, 115 (1974).

²⁴A. Kanda, B. J. Baelus, D. Y. Vodolazov, J. Berger, R. Furugen, Y. Ootuka, and F. M. Peeters, *Phys. Rev. B* **76**, 094519 (2007).

²⁵D. Y. Vodolazov, F. M. Peeters, T. T. Hongisto, and K. Y. Arutyunov, *Europhys. Lett.* **75**, 315 (2006).

²⁶D. Y. Vodolazov, B. J. Baelus, and F. M. Peeters, *Phys. Rev. B* **66**, 054531 (2002).

²⁷R. S. Newbower, M. R. Beasley, and M. Tinkham, *Phys. Rev. B* **5**, 864 (1972).

²⁸K. Arutyunov, D. Golubev, and A. Zaikin, *Phys. Rep.* **464**, 1 (2008).

²⁹V. Ambegaokar and U. Eckern, *Phys. Rev. B* **44**, 10358 (1991).

³⁰V. Ambegaokar and U. Eckern, *Europhys. Lett.* **13**, 733 (1990).

³¹F. von Oppen and E. K. Riedel, *Phys. Rev. B* **46**, 3203 (1992).

³²G. Schwiete and Y. Oreg, *Phys. Rev. Lett.* **103**, 037001 (2009).

³³H. Bluhm, N. C. Koshnick, M. E. Huber, and K. A. Moler, *Phys. Rev. Lett.* **97**, 237002 (2006).

³⁴N. Byers and C. N. Yang, *Phys. Rev. Lett.* **7**, 46 (1961).

³⁵X. Zhang, Ph.D. thesis, University of Colorado, 1996.

³⁶D. J. Scalapino, M. Sears, and R. A. Ferrell, *Phys. Rev. B* **6**, 3409 (1972).

³⁷*The Physics of Superconductors*, Vol. 2, edited by K. H. Bennemann and J. B. Ketterson (Springer, Berlin, 2004), p. 775.

³⁸S. Bell, *J. Phys. B* **3**, 745 (1979).

³⁹P. G. Bjornsson, B. W. Gardner, J. R. Kirtley, and K. A. Moler, *Rev. Sci. Instrum.* **72**, 4153 (2001).

⁴⁰M. E. Huber, N. C. Koshnick, H. Bluhm, L. J. Archuleta, T. Azua, P. G. Björnsson, B. W. Gardner, S. T. Halloran, E. A. Lucero, and K. A. Moler, *Rev. Sci. Instrum.* **79**, 053704 (2008).

⁴¹M. Tinkham, *Introduction to Superconductivity*, 2nd ed. (Dover, New York, 2004).

⁴²M. E. Huber, P. A. Neil, R. G. Benson, D. A. Burns, A. F. Corey, C. S. Flynn, Y. Kitaygorodskaya, O. Massihzadeh, J. M. Martinis, and G. C. Hilton, *IEEE Trans. Appl. Supercond.* **11**, 4048 (2001).

⁴³J. J. Hauser, *J. Low Temp. Phys.* **7**, 335 (1972).

⁴⁴K. A. Matveev, A. I. Larkin, and L. I. Glazman, *Phys. Rev. Lett.* **89**, 096802 (2002).